Formation of Ge nanoparticles in SiO_XN_Y by ion implantation and thermal annealing

S. Mirzaei' , F. Kremer, D. J. Sprouster, L. L. Araujo, R. Feng, C. J. Glover, and M. C. Ridgway

Citation: Journal of Applied Physics **118**, 154309 (2015); doi: 10.1063/1.4933396
View online: http://dx.doi.org/10.1063/1.4933396
View Table of Contents: http://aip.scitation.org/toc/jap/118/15
Published by the American Institute of Physics

Formation of Ge nanoparticles in SiO_xN_y by ion implantation and thermal annealing

S. Mirzaei,[1,a)] F. Kremer,[1] D. J. Sprouster,[2] L. L. Araujo,[3] R. Feng,[1] C. J. Glover,[4] and M. C. Ridgway[1]

[1]*Department of Electronic Materials Engineering, Australian National University, Canberra 0200, Australia*
[2]*Nuclear Science and Technology Department, Brookhaven National Laboratory, Upton, New York 11973, USA*
[3]*Laboratório de Implantação Iônica, Instituto de Física, Universidade Federal do Rio Grande do Sul, Porto Alegre, RS 91501-970, Brasil*
[4]*Australian Synchrotron, 800 Blackburn Road, Clayton, Melbourne, Australia*

(Received 14 July 2015; accepted 7 October 2015; published online 20 October 2015)

Germanium nanoparticles embedded within dielectric matrices hold much promise for applications in optoelectronic and electronic devices. Here we investigate the formation of Ge nanoparticles in amorphous $SiO_{1.67}N_{0.14}$ as a function of implanted atom concentration and thermal annealing temperature. Using x-ray absorption spectroscopy and other complementary techniques, we show Ge nanoparticles exhibit significant finite-size effects such that the coordination number decreases and structural disorder increases as the nanoparticle size decreases. While the composition of $SiO_{1.67}N_{0.14}$ is close to that of SiO_2, we demonstrate that the addition of this small fraction of N yields a much reduced nanoparticle size relative to those formed in SiO_2 under comparable implantation and annealing conditions. We attribute this difference to an increase in an atomic density and a much reduced diffusivity of Ge in the oxynitride matrix. These results demonstrate the potential for tailoring Ge nanoparticle sizes and structural properties in the SiO_xN_y matrices by controlling the oxynitride stoichiometry. © *2015 AIP Publishing LLC*. [http://dx.doi.org/10.1063/1.4933396]

INTRODUCTION

Semiconductor nanoparticles (NPs) are novel material systems that lie between the molecular and solid-state regimes, exhibiting unique properties controlled by their size and structure.[1] Their exceptional optical and electrical characteristics make them ideal for optoelectronic and non-volatile memory devices.[2] Of particular interest are Ge NPs embedded in a dielectric matrix due to their ability to both emit light[3] and store charge.[4] A common and effective way of forming NPs in dielectric matrices is ion implantation where interactions between the implanted atoms and the host matrix are crucial in determining the final state of the NPs.[5] The matrix thus has a significant influence on the properties of the NPs formed therein. For example, Si NPs of equal size exhibit different bandgaps in SiO_2 and Si_3N_4.[6]

The growth and characterization of Ge NPs embedded in a SiO_2 matrix, and to a lesser extent Si_3N_4, have been previously reported.[7–15] However, the formation of Ge NPs in SiO_xN_y matrices by ion implantation has not been studied extensively. As a matrix, SiO_xN_y is potentially advantageous relative to SiO_2 and Si_3N_4 given the ability to manipulate the NP properties by varying the matrix stoichiometry. For example, Ehrhardt *et al.*[6] reported the size of Si NPs in Si-rich SiO_xN_y was governed by the Si excess. Mirabella *et al.*[15] reported the size of the Ge NPs was smaller in Si_3N_4 compared to SiO_2 as attributed to a reduced Ge diffusivity in the nitride. In this study, we investigate the size and structural properties of the Ge NPs formed in the amorphous $SiO_{1.67}N_{0.14}$ by ion implantation and thermal annealing. We chose an oxynitride stoichiometry close to that of SiO_2 to demonstrate the significant influence of a small fraction of N on the size and structural properties of the Ge NPs.

The synchrotron-based techniques of x-ray absorption near-edge structure (XANES) and extended x-ray absorption fine-structure (EXAFS) were used to characterize the NP structural properties. The crystalline and amorphous fractions were determined with XANES while the structural parameters of the nearest-neighbor (NN) shell were determined with an EXAFS. These results were supplemented by Rutherford backscattering spectrometry (RBS), transmission electron microscopy (TEM), and Raman spectrometry measurements. RBS was used to measure the depth distribution of Ge atoms, TEM to determine the NP size distribution and Raman spectroscopy to support the XANES results. Using this combination of complementary techniques, we achieve a detailed picture of the size-dependent structural properties of Ge NPs and show they are governed by finite-size effects.

EXPERIMENTAL PROCEDURES

An amorphous $SiO_{1.67}N_{0.14}$ layer of thickness $\sim 1\,\mu$m was deposited on a Si (100) substrate by plasma-enhanced chemical vapor deposition with the stoichiometry deduced by the RBS. With this technique, the H content is typically $\sim$1–5 at. % as-deposited, decreasing to a negligible fraction after annealing above 1100 °C.[16,17] ^{74}Ge ions were implanted into the $SiO_{1.67}N_{0.14}$ layer at an energy of 700 keV to the fluences of either 2.7 or $3.3 \times 10^{17}\,cm^{-2}$. To promote *in-situ* NP nucleation and growth, the substrate was maintained at

a)sahar.mirzaei@anu.edu.au

400 °C during implantation. Samples were then annealed for 1 h in a N_2 ambient at 700, 900, or 1100 °C.

RBS measurements were performed with 4.5 MeV He^{2+} ions and a Si surface-barrier detector positioned at a scattering angle of 168°. The use of this energy enabled the complete separation of the Ge depth distribution from the substrate signal extending from the surface to the oxynitride/substrate interface. RBS spectra were analyzed with the RUMP program.[18]

Cross-sectional TEM images were obtained in bright-field mode using a JEOL 2100 F microscope operated at 200 kV. Samples were prepared using a standard ion-beam-milling protocol.

Raman spectroscopy was performed with a Jobin-Yvon Horiba T64000 spectrometer operating in the single spectrometer mode (resolution $> 1\,cm^{-1}$) using a liquid N_2 cooled CCD detector in the backscattering configuration. Spectra were acquired at room temperature using a short working distance objective (Nikon, 100×) and a HeNe laser (632.8 nm) focused on a 2 μm diameter spot. Ten spectra per sample were collected from various locations and averaged. The common Raman artefact near $\sim 300\,cm^{-1}$ (Refs. 12 and 19) resulting from the overlap of the transverse-acoustic second-order phonon mode of Si-Si bonds and the longitudinal-optical first-order phonon mode of Ge-Ge bonds was completely eliminated by removing the Si substrate below the $SiO_{1.67}N_{0.14}$ layer as described in the next paragraph and thus no special measurement geometries were required.

XANES and EXAFS measurements were performed at the Ge K-edge (11.103 keV) and a temperature of 15 K using the x-ray absorption spectroscopy beamline of the Australian Synchrotron. Fluorescence spectra were recorded with a 10 × 10 Ge pixel-array detector. Data were collected to a photoelectron wavenumber (k) of 15 $Å^{-1}$. For energy calibration, a crystalline Ge (c-Ge) reference foil was simultaneously measured in the transmission mode. To improve the signal-to-noise ratio and enable high-resolution measurements, the Si substrate below the $SiO_{1.67}N_{0.14}$ layer was removed by mechanical grinding and selective chemical etching with KOH.[20,21] The Ge-implanted $SiO_{1.67}N_{0.14}$ layers were then stacked together and mounted between Kapton in an Al frame.[22] A bulk amorphous Ge (a-Ge) sample was prepared by ion implantation as described elsewhere.[23]

Absorption spectra were first averaged with the program AVERAGE[24] then processed and analyzed with ATHENA and ARTEMIS.[25] After background subtraction using the AUTOBK algorithm implemented in ATHENA,[25] data were then Fourier transformed (FT) using a Hanning window of width 4.1 to 13.5 $Å^{-1}$ in k space. In back transforming from radial distance (r) space, a Hanning window of width 1.4–2.8 Å was utilized. Values of the energy shift parameter ΔE_0 were defined using ARTEMIS and by following the procedure suggested in Ref. 26 to align the k scale of the theoretical standard for all samples as well as to avoid distortions in the structural parameters arising from a poor choice of the edge energy position (E_0). Effective scattering amplitudes and phase shifts were calculated *ab initio* with FEFF8.[27] Spectra were fitted with a single-scattering path about the Ge absorber to probe the structural parameters of the NN shell using the fitting procedure suggested in Refs. 28–31. For the bulk c-Ge standard, the values of S_0^2 and ΔE_0 were 0.93 ± 0.08 and 3.84 ± 0.93 eV, respectively. These values were then fixed for the fitting of all remaining samples. Coordination numbers (CN) were fixed to four for the bulk c-Ge standard and fitted for a-Ge and the Ge NPs. The inter-atomic distances (R), Debye-Waller factors (DWF) (σ^2), and asymmetry in the distribution of inter-atomic distances (C_3) were determined. Each data set was fitted with multiple k-weightings ranging from 1 to 4.

RESULTS AND DISCUSSION

The depth distribution of implanted Ge atoms in the amorphous $SiO_{1.67}N_{0.14}$ layer was measured by the RBS before and after thermal annealing, an example of which is shown in Figure 1. In an as-implanted state, the peak concentrations for the two different implantation fluences were ∼9 and ∼12 at. % and were centered at a depth of ∼0.3 μm with a full width at half maximum of ∼0.3 μm. The depth of the concentration maximum determined by the RBS agreed with the TRIM predictions.[32] Figure 1 demonstrates that thermal annealing did not lead to a significant loss or redistribution of Ge atoms consistent with the non-diffusive, non-reactive model of Heinig *et al.*[33] which correlates the lack of redistribution to the absence of H_2O and O_2. Similar observations have been reported for Ge NPs formed in SiO_2.[29,34] Acquiring the spectra at the energy of 4.5 MeV resulted in the appearance of nuclear resonances from different isotopes of N, O, and Si. The presence of multiple resonances impedes accurate normalization. Both spectra were normalized at the low-medium energy end of the spectrum, below the energy of the resonances.

Representative TEM images and NP size distributions are shown in Figure 2. Spherical, crystalline NPs were observed in all annealed samples. High resolution images are shown in the insets and (111) lattice planes of the Ge diamond cubic structure are discernible. The size distributions are Gaussian-like. Mean NP diameters were calculated by averaging the NP volume through cubic weighting of the

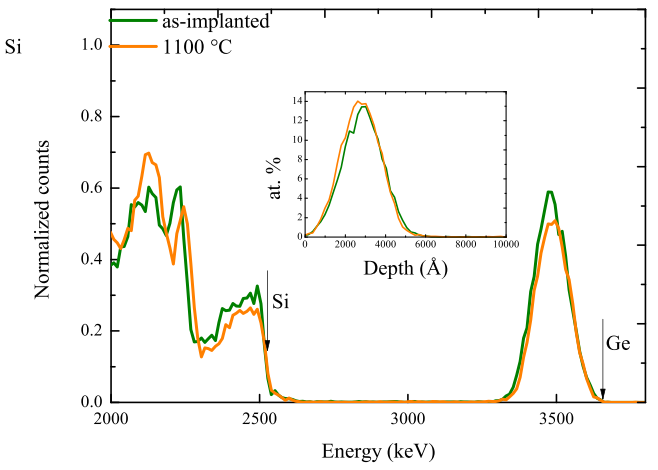

FIG. 1. RBS spectra before and after annealing (1100 °C/1 h) for samples of 12 at. % Ge. Arrows indicate Si and Ge surface energies (2512 and 3658 keV, respectively).

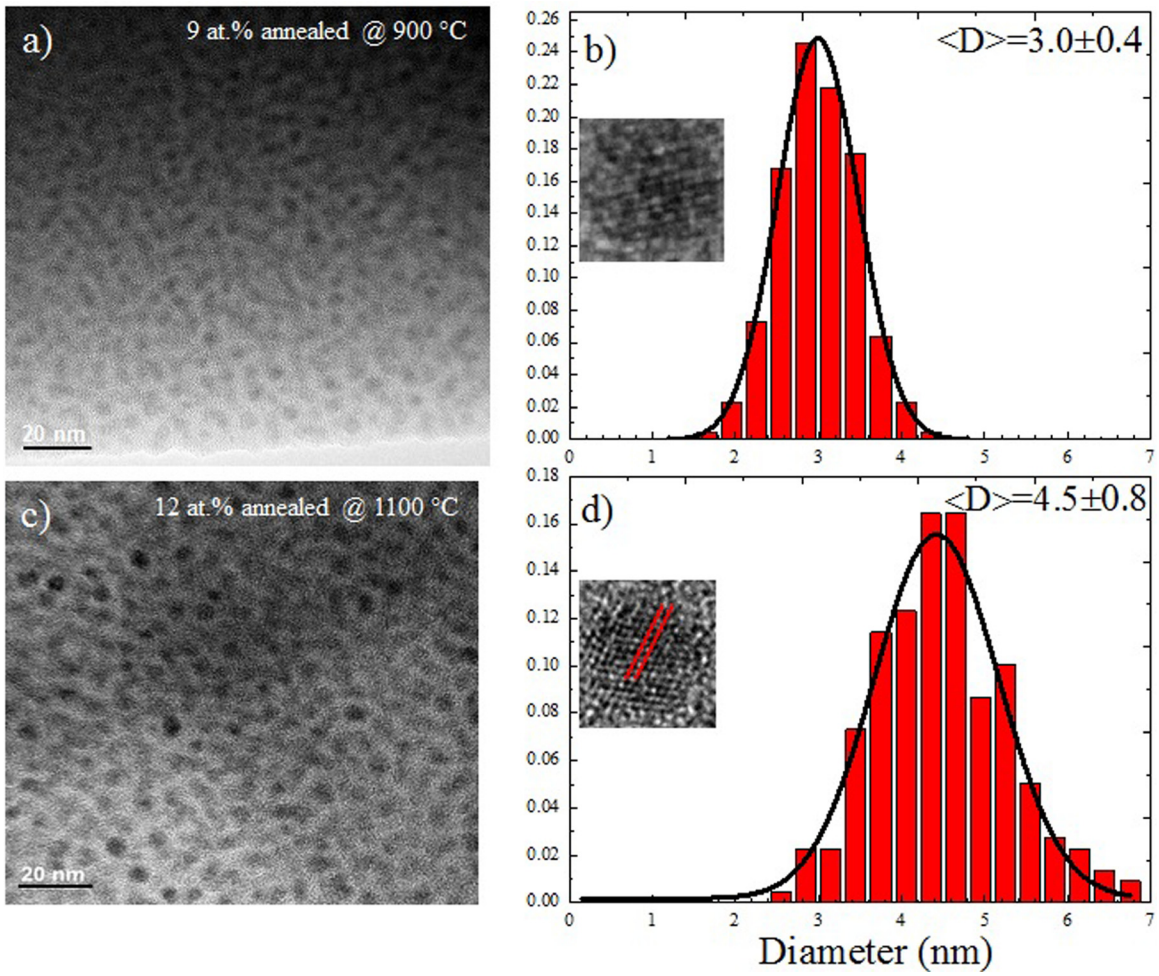

FIG. 2. TEM images recorded near the Ge concentration maximum for 9 at. % Ge 900 °C and 12 at. % Ge/1100 °C samples with the respective NP size distributions.

extracted NP diameters. Results are listed in Table I. Clearly, the NP size increases as the annealing temperature and/or Ge concentration increase. In comparison with Ge NPs formed under comparable conditions in SiO_2,[22,29] we have shown that the Ge concentration of both 3 and 10 at. % results in the formation of large crystalline Ge NPs. For common combinations of annealing temperature and time (1100 °C, 1 h), the NP sizes determined in SiO_2 (10 at. %: 14 nm, 3 at. %: 6.4 nm) are significantly larger than those determined here for $SiO_{1.67}N_{0.14}$ with higher Ge concentrations (9 at. %: 3.7 nm, 12 at. %: 4.5 nm). Ge NPs formed in $SiO_{1.67}N_{0.14}$ are considerably smaller, indicative of a slower rate of NP growth. The $SiO_{1.67}N_{0.14}$ matrix thus has a non-negligible effect on inhibiting the diffusion of the high concentration of Ge atoms, and retarding the growth of NPs. The latter may well result from a reduced Ge diffusivity in

TABLE I. NP size and structural parameters as a function of implantation fluence and annealing temperature (R-factor from 0.0029 to 0.0034).

Sample	Annealing temp. (°C)	NP size (nm)	CN (atoms)	R (Å)	σ^2 (10^{-3} Å^2)	C_3 (10^{-4} Å^3)
c-Ge	…		4	2.445 ± 0.001	2.5 ± 0.2	0.0 ± 0.3
3 at. %[a]	1100	6.4 ± 0.3	3.7 ± 0.2	2.441 ± 0.003	3.1 ± 0.2	0.7 ± 0.3
10 at. %[b]	1100	14 ± 0.7	3.9 ± 0.14	2.443 ± 0.002	2.7 ± 0.1	1.86 ± 1.6
9 at. %[c]	900	3.0 ± 0.4	3.3 ± 0.3	2.452 ± 0.004	4.4 ± 0.5	0.0 ± 0.6
	1100	3.7 ± 0.7	3.5 ± 0.1	2.457 ± 0.005	4.1 ± 0.7	0.0 ± 0.7
12 at. %[c]	900	4.1 ± 0.7	3.5 ± 0.3	2.446 ± 0.008	3.8 ± 0.4	0.0 ± 1.1
	1100	4.5 ± 0.8	3.6 ± 0.2	2.451 ± 0.005	3.7 ± 0.7	0.0 ± 0.7
a-Ge	…		3.9 ± 0.2	2.447 ± 0.004	4.5 ± 0.2	−0.3 ± 0.7

[a]SiO_2 Ref. 29
[b]SiO_2 Ref. 22
[c]$SiO_{1.67}N_{0.14}$ this work

TABLE II. Bond energies for Si- and Ge- bonds.[35]

System	kJ/mol	system	kJ/mol
Si-N	437	Ge-N	395
Si-O	799	Ge-O	658
Si-Si	310	Ge-Si	297
Si-Ge	297	Ge-Ge	264

$SiO_{1.67}N_{0.14}$ compared to SiO_2, consistent with the observations of Mirabella *et al*. for Si_3N_4.[15] Indeed, no evidence of the Ge diffusion was apparent in the RBS spectra presented earlier. Given diffusion necessitates bond breaking, the strong covalent bonds in SiO_2 and Si_3N_4 clearly do not favor diffusion in either the oxide or nitride. (see Table II for a listing of bond energies[35]). The two matrices also differ considerably in atomic density (6.82×10^{22} and 1.03×10^{23} atoms/cm^3, respectively) and the greater number of bonds per unit volume in the nitride may further impede diffusion. Furthermore, the three bonds connected to each N in Si_3N_4 are more constrained than the two bonds of each O atom in SiO_2 where the Si-O-Si bond angles can range from 120° to 180° with little change in energy.[36] These more constrained bonds are another important reason for the reduced diffusivity in the nitrided lattices.[36]

The amorphous and crystalline phase fractions of the Ge NPs were determined with the XANES. Representative spectra are shown in Figure 3 for the 12 at. % Ge samples as a function of annealing temperature. The spectra much more closely resemble that of c-Ge than a-Ge from which we infer that the phase fraction of an amorphous component is minimal at most. Equivalently, the c-Ge like features of the NP spectra demonstrate the phase fraction of a crystalline component is dominant. Indeed, linear combination fitting indicated an amorphous fraction was negligible consistent with the TEM observations presented above. Also, no evidence of Ge nitride, oxide, or silicide formation was apparent from the XANES analysis. The Ge-only composition of the NPs is consistent with the TEM results and also bond energy values as given in Table II. While Si and Ge are completely miscible and readily alloy, clearly Si preferentially bonds to O and N.

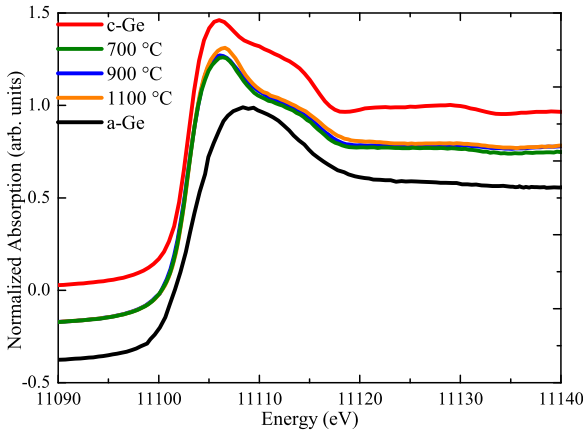

FIG. 3. XANES spectra for 12 at. % Ge samples as a function of annealing temperature (700, 900 and 1100 °C) plus crystalline and amorphous standards. The spectra are offset vertically for clarity.

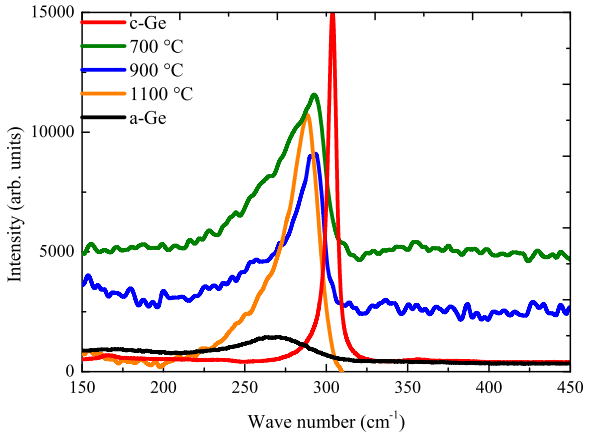

FIG. 4. Raman spectra for 12 at. % Ge samples as a function of annealing temperature (700, 900 and 1100 °C) plus crystalline and amorphous standards. The spectra are offset vertically for clarity.

Raman spectra are shown in Figure 4 for the 12 at. % Ge samples as a function of annealing temperature. As discussed previously, there is no interference from the second-order Raman peak from Si due to the sample preparation method. Relative to the crystalline standard, peak broadening, a redshift, and asymmetry are observed. The broadening of the NP Ge-Ge mode is the result of structural disorder while the redshift can be attributed to compressive strain and/or an isotopic effect.[37] The asymmetric broadening is the result of finite-size effects.[38] Scattering contributions from crystalline Ge-Si were not apparent as consistent with the XANES results. The presence of an a-Ge phase fraction could contribute to the observed peak broadening. However, no evidence of an amorphous phase component was apparent with the XANES as noted previously.

The structural parameters of the first NN shell surrounding a Ge atom were determined with EXAFS. Figures 5(a) and 5(c) show isolated k^3-weighted EXAFS

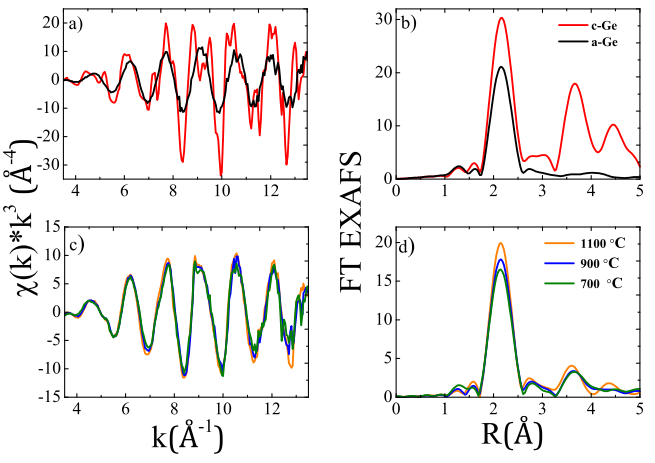

FIG. 5. Top: (a) Raw EXAFS oscillations and (b) Fourier-transformed EXAFS signal for bulk c-Ge and a-Ge standards. Bottom: (a) Raw EXAFS oscillations and (b) Fourier-transformed EXAFS signal for 9 at. % Ge samples as a function of annealing temperature.

while Figures 5(b) and 5(d) show the FT spectra of the standards and samples with a Ge concentration of 9 at. %. The refined fitting parameters for the first NN shell are listed in Table I. For the crystalline and amorphous bulk standards, the EXAFS spectra shown in Figure 5(a) are the result of scattering from multiple and single atomic shells surrounding a Ge atom, respectively. Indeed, for the a-Ge, no scattering contribution from beyond the first NN shell is evident in the FT spectrum of Figure 5(b), consistent with the structural disorder inherent in the amorphous phase. In contrast, scattering contributions from the first, second, and third NN shells are apparent for the c-Ge, consistent with the diamond cubic structure. For the NP samples, the amplitude of the first NN peak decreases as the annealing temperature decreases. This is the result of the decrease in size and, hence, the increase in the surface-area-to-volume ratio, yielding both a reduction in average coordination number and an increase in structural disorder. The latter is due to bonding distortions at or near the NP/matrix interface.[39] The near-zero value of C_3 is indicative of a lack of asymmetry in the inter-atomic distance distribution. The decrease in the CN and increase in the DWF are both characteristics of the so-called finite-size effects as the surface-area-to-volume ratio increases. Structurally, Ge NPs in $SiO_{1.67}N_{0.14}$ are thus similar to those in SiO_2. Interestingly, the matrix does not appear to have any effect on the structural properties of the NPs, with the CN, BL, and DWF quantified here in agreement with the size dependent trends previously observed for Ge NPs in SiO_2.[29] The most striking difference is the decrease in the NP size observed in the oxynitride which again demonstrates the very significant influence of matrix composition on the size distribution of Ge NPs formed by ion implantation and thermal annealing. The size of the Ge NPs can thus be controlled by the very slight addition of N to a nominally oxide matrix.

CONCLUSION

In summary, we have utilized a variety of complementary analytical techniques to characterize Ge NPs formed in $SiO_{1.67}N_{0.14}$ by ion implantation and thermal annealing. The Ge NPs were single-crystalline and diamond cubic in structure with finite-size effects readily measureable. The NP size was dependent on both the implantation fluence and annealing temperature. For comparable implantation and annealing conditions, Ge NPs formed in $SiO_{1.67}N_{0.14}$ were smaller in size than those formed in SiO_2 demonstrating the influence of matrix composition. We attribute this difference to an increase in density and a relative decrease in Ge atom diffusivity in the oxynitride matrix. In general, much of nanotechnology involves the exploitation of finite-size effects for superior device performance and such effects become more pronounced as the NP size decreases. In this report, we have demonstrated that a small fraction of N in an oxynitride matrix yields smaller NPs than in a pure oxide matrix, a result of both scientific importance and technological relevance.

ACKNOWLEDGMENTS

We acknowledge access to NCRIS infrastructure at the Australian National University including the Australian National Fabrication Facility and the Heavy Ion Accelerator Capability. We also thank the Australian Research Council and Australian Synchrotron for support. Access to the facilities of the Centre for Advanced Microscopy, with funding through the Australian Microscopy and Microanalysis Research Facility, is gratefully acknowledged.

[1]E. Roduner, Chem. Soc. Rev. **35**, 583 (2006).
[2]S. K. Ray, S. Maikap, W. Banerjee, and S. Das, J. Phys. D: Appl. Phys. **46**, 153001 (2013).
[3]S. K. Ray and K. Das, Opt. Mater. **27**, 948 (2005).
[4]C. J. Park, K. H. Cho, W. C. Yang, H. Y. Cho, S. H. Choi, R. G. Elliman, J. H. Han, and C. Kim, Appl. Phys. Lett. **88**, 071916 (2006).
[5]A. Meldrum, R. F. Haglund, L. A. Boatner, and C. W. White, Adv. Mater. **13**, 1431 (2001).
[6]F. Ehrhardt, G. Ferblantier, D. Muller, C. Ulhaq-Bouillet, H. Rinnert, and A. Slaoui, J. Appl. Phys. **114**, 033528 (2013).
[7]J. G. Zhu, C. W. White, J. D. Budai, S. P. Withrow, and Y. Chen, J. Appl. Phys. **78**, 4386 (1995).
[8]A. Markwitz, L. Rebohle, H. Hofmeister, and W. Skorupa, Nucl. Instrum. Methods Phys. Res., Sect. B **147**, 361 (1999).
[9]A. J. Williamson, C. Bostedt, T. van Buuren, T. M. Willey, L. J. Terminello, G. Galli, and L. Pizzagalli, Nano Lett. **4**, 1041 (2004).
[10]V. Cantelli, J. von Borany, A. Mucklich, and N. Schell, Nucl. Instrum. Methods Phys. Res., Sect. B **238**, 268 (2005).
[11]J. S. Jensen, T. P. L. Pedersen, R. Pereira, J. Chevallier, J. L. Hansen, B. B. Nielsen, and A. N. Larsen, Appl. Phys. A: Mater. Sci. Process. **83**, 41 (2006).
[12]A. Wellner, V. Paillard, C. Bonafos, H. Coffin, A. Claverie, B. Schmidt, and K. H. Heinig, J. Appl. Phys. **94**, 5639 (2003).
[13]M. Derivaz, P. Noé, D. Jalabert, J. L. Rouviére, D. Buttard, D. Sotta, and A. Barski, Microelectron. Eng. **61–62**, 643 (2002).
[14]S. Lee, S. Huang, G. Conibeer, and M. A. Green, Energy Procedia **10**, 20 (2011).
[15]S. Mirabella, S. Cosentino, A. Gentile, G. Nicotra, N. Piluso, L. V. Mercaldo, F. Simone, C. Spinella, and A. Terrasi, Appl. Phys. Lett. **101**, 011911 (2012).
[16]K. Worhoff, E. Klein, G. Hussein, and A. Driessen, in *Proceedings of the 10th International Conference on Transparent Optical Networks*, Athens, Greece, June 22–26, edited by M. Marciniak (IEEE, Athens, 2008), pp. 266–269.
[17]M. G. A. W. Hussein, K. A. Roeloffzen, C. G. H. A. Hilderink, L. T. H. A. Ridder, and R. M. A. de Driessen, in *Proceedings of IEEE/LEOS Benelux Chapter 2001 Annual Symposium* (VUB Press, Brussel, 2001).
[18]L. R. Doolittle, Nucl. Instrum. Methods Phys. Res., Sect. B **9**, 344 (1985).
[19]A. V. Kolobov, J. Appl. Phys. **87**, 2926 (2000).
[20]L. C. Chen, M. J. Chen, C. C. Wan, T. H. Tsaur, and C. S. Lien, Mater. Sci. Eng. B **34**, 180 (1995).
[21]S. Decoster, C. J. Glover, B. Johannessen, R. Giulian, D. J. Sprouster, P. Kluth, L. L. Araujo, Z. S. Hussain, C. Schnohr, H. Salama, F. Kremer, K. Temst, A. Vantomme, and M. C. Ridgway, J. Synchrotron Radiat. **20**, 426 (2013).
[22]A. Cheung, G. D. Azevedo, C. J. Glover, D. J. Llewellyn, R. G. Elliman, G. J. Foran, and M. C. Ridgway, Appl. Phys. Lett. **84**, 278 (2004).
[23]M. C. Ridgway, G. D. Azevedo, R. G. Elliman, C. J. Glover, D. J. Llewellyn, R. Miller, W. Wesch, G. J. Foran, J. Hansen, and A. Nylandsted-Larsen, Phys. Rev. B **71**, 094107 (2005).
[24]J. Hester, see http://www.synchrotron.org.au/aussyncbeamlines/x-ray-absorption-spectroscopy/data-analysis.
[25]B. Ravel and M. Newville, J. Synchrotron Radiat. **12**, 537 (2005).
[26]S. D. Kelly and B. Ravel, AIP Conf. Proc. **882**, 132–135 (2007).
[27]J. J. Rehr and R. C. Albers, Rev. Mod. Phys. **72**, 621 (2000).
[28]L. L. Araujo, G. J. Foran, and M. C. Ridgway, J. Phys.: Condens. Matter **20**, 165210 (2008).
[29]L. L. Araujo, R. Giulian, D. J. Sprouster, C. S. Schnohr, D. J. Llewellyn, P. Kluth, D. J. Cookson, G. J. Foran, and M. C. Ridgway, Phys. Rev. B **78**, 094112 (2008).
[30]L. L. Araujo, P. Kluth, G. D. M. Azevedo, and M. C. Ridgway, Nucl. Instrum. Methods Phys. Res., Sect. B **257**, 56 (2007).
[31]L. L. Araujo, P. Kluth, and M. C. Ridgway, Phys. Rev. B **74**, 184102 (2006).
[32]J. Ziegler, J. P. Beirsack, and U. Littmark, *The Stopping and Range of Ions in Matter* (Pergamon, New York, 1985).

[33]K. H. Heinig, B. Schmidt, A. Markwitz, R. Grotzschel, M. Strobel, and S. Oswald, Nucl. Instrum. Methods Phys. Res., Sect. B **148**, 969 (1999).
[34]G. E. J. Koops, H. Pattyn, A. Vantomme, S. Nauwelaerts, and R. Venegas, Phys. Rev. B **70**, 235410 (2004).
[35]Y.-R. Luo, *Comprehensive Handbook of Chemical Bond Energies* (CRC Press, Boca Raton, 2012).
[36]B. E. Deal and C. R. Helms, *The Physics and Chemistry of SiO2 and the Si-SiO2 Interface* (Springer, New York, USA, 1993), p. 187.
[37]M. Cardona and M. L. W. Thewalt, Rev. Mod. Phys. **77**, 1173 (2005).
[38]M. Fujii, S. Hayashi, and K. Yamamoto, Appl. Phys. Lett. **57**, 2692 (1990).
[39]M. Backman, F. Djurabekova, O. H. Pakarinen, K. Nordlund, L. L. Araujo, and M. C. Ridgway, Phys. Rev. B **80**, 144109 (2009).